



Fano test, clinical proton beams and nuclear reactions

J.A. de la Torre^{a,b}, A.M. Lallena^{a,b} , M. Anguiano^{a,b,*}

^a Departamento de Física Atómica, Molecular y Nuclear, Universidad de Granada, E-18071 Granada, Spain

^b Instituto de Investigación Biosanitaria (ibs.GRANADA), Complejo Hospitalario Universitario de Granada/Universidad de Granada, E-18016 Granada, Spain

ARTICLE INFO

Keywords:

Fano test for proton beams
Monte carlo

PENH
FLUKA
TOPAS

ABSTRACT

Purpose : A Fano test is implemented to prove the feasibility of the Monte Carlo simulation codes PENH, FLUKA and TOPAS for proton transport and, in particular, for the calculation of perturbation factors in ionization chambers used in proton-therapy. Optimal simulation parameters have been determined for PENH and revised for TOPAS and FLUKA.

Methods : Simulations of proton beams with initial energies between 50 and 250 MeV have been performed. Fano test has been checked by locally absorbing secondary particles and switching off nuclear reactions. Particular attention has been paid to the role of the tracking parameters in the verification of the test. Results obtained in previous works have been revisited. The role of radiation production and nuclear reactions has been also investigated.

Results : The results obtained for different materials conforming the simulation phantom indicate that PENH verifies the test if the key parameter W_{ec} takes values of 10 keV at most; in this case other tracking parameters do not affect these findings. FLUKA verifies the test in all the cases analyzed. TOPAS fails to accomplish the Fano test for initial proton energies larger than 100 MeV, even if the optimal values of different tracking parameters suggested in previous publications are used. Nuclear reactions are responsible of most of the radiation yield produced; this yield makes the test to be violated in the three codes.

Conclusions : The Fano test has permitted to establish the optimal values for the tracking parameters in case of PENH. Using these values PENH verifies the test in all cases studied. TOPAS does not verify it for high initial proton energies, irrespective of the combinations of tracking parameters used.

1. Introduction

Monte Carlo simulations have traditionally been used to accurately calculate ionization chamber dose responses for both photons and electron beams (Zink and Wulff, 2008; Wulff et al., 2008; González-Castaño et al., 2009; Muir and Rogers, 2010; Wulff et al., 2010; Zink and Wulff, 2012; Muir et al., 2012; Erazo and Lallena, 2013; Muir and Rogers, 2013; Erazo et al., 2014; Reis and Nicolucci, 2016; Erazo and Lallena, 2016; Erazo et al., 2017; Garví et al., 2024). In these calculations, uncertainties include not only those of type A associated with the statistical character of the Monte Carlo procedure, but also those due to the physical models considered and to the particle transport algorithms. The latter can be assessed using self-consistency tests like the Fano test, which is grounded in the Fano theorem. This theorem states that: “In a medium of a given composition exposed to a uniform flux of primary radiation (such as X-rays or neutrons), the flux of secondary radiation is also uniform and independent of the density of the medium as well as of density variations from point to point” (Fano, 1954a,b; Spencer, 1975). By applying this theorem it is possible to quantify the relative deviation

from the theoretical solution obtained with the Boltzmann transport equation, assuming the conditions of charged particle equilibrium are met.

For electron beams up to 20 MeV, Sempau and Andreo (2006) conducted an analysis on the stability of the electron transport algorithm utilized in the Monte Carlo code PENELOPE concerning variations in step length; their findings revealed a violation of the Fano test by a maximum of 0.1%. Consequently, the authors concluded the imperative requirement for a meticulous selection of transport parameters. This precision is crucial due to the potential impact of surface effects associated with the heterogeneous geometry and small volume of the ionization chambers under investigation.

In case of protons, Fano test enables the assessment of whether specific details in the corresponding Monte Carlo transport algorithms introduce artifacts when small cavities are present in the simulation geometry. Taking this into consideration, Sterpin et al. (2014), Wulff et al. (2018), and Lourenço et al. (2019), who studied proton beam dosimetry for several ionization chambers, incorporated Fano tests to

* Corresponding author.

E-mail addresses: juanalejandro@ugr.es (J.A. de la Torre), lallena@ugr.es (A.M. Lallena), mangui@ugr.es (M. Anguiano).

determine the optimal parameters for simulations conducted with the different Monte Carlo codes used. Sterpin et al. (2014) analyzed the role of the tracking parameters and concluded that both PENH and Geant4 accomplished the Fano cavity test within 0.1% if these tracking parameters were chosen in such a way that the step sizes generated were small enough.

The results of Wulff et al. (2018) indicated that TOPAS verified the test within 0.1%–0.2% depending on the source type considered and proposed optimal tracking parameters. Finally, Lourenço et al. (2019) found that FLUKA passed the test within 0.15% for the set of tracking parameters they selected for their simulations. These verification limits corresponded to relative differences between the results obtained in the simulations for the quantity used to check the test and its predicted theoretical value. However conclusions on the verification of the test can only be drawn taking into account also the uncertainties of the simulation results: it is on the basis of the latter that it can be established whether the relative differences are significant or not and, as a consequence, whether the test is actually passed. However, this analysis is not always carried out in these terms.

A new version of PENH, featuring improvements in physics models, has recently been made available (Salvat and Quesada, 2020, 2021). In this work, the degree of compliance of this new version of PENH with the Fano test has been studied. Furthermore, a comparison with results obtained using the TOPAS (Perl et al., 2012; Faddegon et al., 2020) and FLUKA (Boehlen et al., 2014; Battistoni et al., 2016) codes has been carried out and the transport parameters indicated in the works by Wulff et al. (2018) and Lourenço et al. (2019) have been discussed. In addition, attention has been paid to the role of nuclear reactions and the radiation production in the test verification.

2. Material and methods

2.1. Implementation of the Fano test

The implementation of the Fano test in this study follows a similar approach to that employed in previous works (Sempau and Andreo, 2006; Wulff et al., 2018). It is based on the reciprocity theorem, according to which the absorbed dose in the detector can be calculated either by considering a small detector irradiated with a broad beam or a large detector irradiated by a small beam (Bielajew and Rogers, 1988). It is worth noting that this theorem has been used as a particular variance reduction technique in some simulations of the kind carried out in the work by Sempau and Andreo (2006).

In the simulations conducted here to validate the Fano test, instead of a phantom irradiated with an external, wide enough, beam, a source inside the phantom has been considered. Under these circumstances, the entire setup must verify three conditions for the correct implementation of the test: (i) the spectral and angular distributions of the emitted particles must be the same at any emission point of the source; (ii) the radiation transport medium must be uniform with respect to its atomic composition and interaction properties, and (iii) the number of emitted particles per unit mass must be constant.

The simulation geometry used in the present work is illustrated in Fig. 1. It consists of three vertically stacked cylinders with a common radius r . The upper and lower ones, referred to as *walls*, have a height h_w , while the central cylinder, identified as the *cavity*, has a height h_c . A linear source, depicted in blue in the figure, emits protons of given initial energy, E_0 , in the direction of the positive z -axis, as indicated by the arrows. This setup fulfills the first condition. Proton beams with energies of 50, 100, 150, 200 and 250 MeV have been considered. In what follows, the source of the setup just described is named “*linear source*”.

A second source type has been also considered in order to compare with previous results. In that case the simulation setup is the same as described above but protons are emitted isotropically in all directions

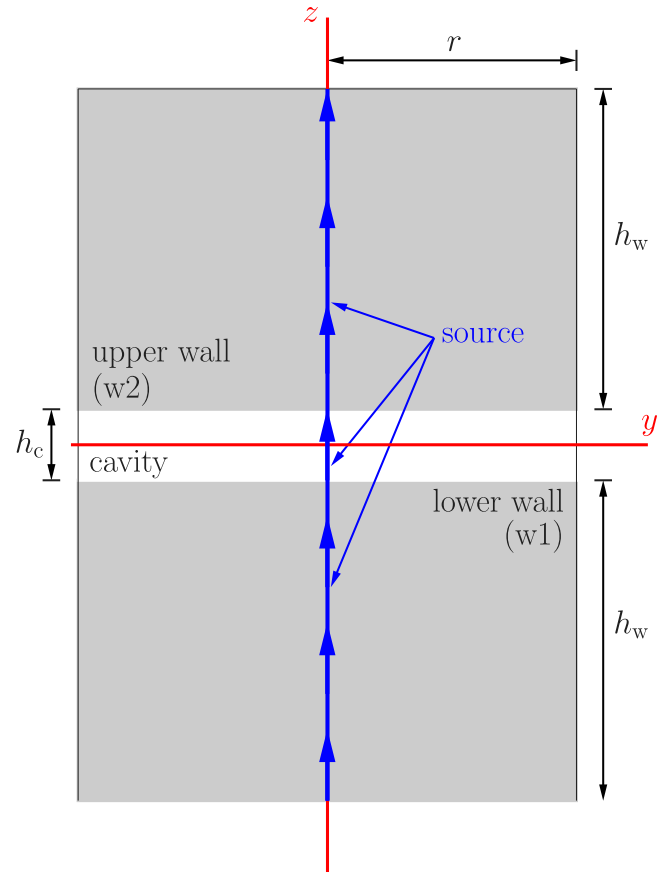


Fig. 1. Geometry considered to implement the Fano test in the present work. The scheme corresponds to the so-called “linear source” (see text).

Table 1

Values of the height h_w , as given by Eq. (1), of the walls of the phantom used for the various energies analyzed. N_w indicates the number of initial protons emitted from each of the two walls in the various simulations for the two sources, linear and isotropic, considered.

Energy (MeV)	h_w (cm)			N_w	
	Al	Water	C	Linear	Isotropic
50.	1.52	3.12	1.75	$1.3 \cdot 10^8$	$3.0 \cdot 10^8$
100.	5.19	10.81	6.07	$3.0 \cdot 10^8$	$4.5 \cdot 10^8$
150.	10.54	22.08	12.41	$5.0 \cdot 10^8$	$6.5 \cdot 10^8$
200.	17.28	36.34	20.42	$7.0 \cdot 10^8$	$8.0 \cdot 10^8$
250.	25.18	53.12	28.89	$1.0 \cdot 10^9$	$1.0 \cdot 10^9$

instead of only in the positive z -direction as in the linear source. This second source is named “*isotropic source*” in what follows.

As the verification of the Fano test is carried out in the cavity, it is essential to ensure charged particle equilibrium in this region. Following the advice of Sempau and Andreo (2006), the value of h_w must exceed the continuous slowing down approximation range of protons with initial energy E_0 , in the material fulfilling the walls, $R(E_0)$. In our simulations we have chosen

$$h_w(E_0) = 1.4 \cdot R(E_0) = 1.4 \cdot R_\rho(E_0)/\rho, \quad (1)$$

where $R_\rho(E_0)$ represents the corresponding mass range of protons with energy E_0 in a material of density ρ . The $R_\rho(E_0)$ values have been taken from Berger et al. (2017).

To study the optimal tracking parameters for PENH, we have chosen Al because of its well-established characteristic parameters: $I = 166$ eV and $\rho = 2.6989$ g cm⁻³. The values of h_w used for the various proton energies considered are given in Table 1.

The cavity has been filled with a fictitious material, with the same composition as Al and a density $\rho_c = 0.001 \text{ g cm}^{-3}$. This design permits to meet the second condition and, in addition, emulates the configuration of a typical ionization chamber, usually filled with air or other gases. For the height of the cavity we have used $h_c = 0.2 \text{ cm}$. Finally, we have considered $r = 10 \cdot h_w$ (250 MeV) for all proton energies studied.

To compare with previous results, and to check the optimal parameters proposed for TOPAS (Wulff et al., 2018) and FLUKA (Lourenço et al., 2019), additional simulations have been conducted, wherein Al has been replaced by water and C. In these calculations, the values of the parameters defining the simulation geometry have been chosen by following the same prescriptions as in the case of Al, taking into account that $I = 78 \text{ eV}$ and $\rho = 1.0 \text{ g cm}^{-3}$ for water and $I = 81 \text{ eV}$ and $\rho = 2.0 \text{ g cm}^{-3}$ for C (see Table 1).

The third condition requires the determination of the probability of a proton being emitted as a function of the emission point, ensuring the constancy of the number of particles emitted per unit mass. Let N_{w1} , N_{w2} and N_{cav} the number of protons emitted from the source piece embedded in each of the two walls and in the cavity, respectively. The condition to be satisfied imposes that:

$$\frac{N_{\text{wall}}}{m_w} = \frac{N_{\text{cav}}}{m_c}, \quad (2)$$

where m_w denotes the mass of each wall, m_c that of the cavity and it has been assumed that $N_{w1} = N_{w2} = N_{\text{wall}}$. Taking into account the densities of the wall and cavity materials, one has:

$$N_{\text{cav}} = \frac{\rho_c h_c}{\rho_w h_w} N_{\text{wall}}. \quad (3)$$

The total number of protons emitted is then:

$$N_{\text{tot}} = 2 N_{\text{wall}} + N_{\text{cav}} = \left(2 + \frac{\rho_c h_c}{\rho_w h_w} \right) N_{\text{wall}}. \quad (4)$$

The proton emission probabilities in the three cylinders composing the geometry are easily obtained from Eqs. (3) and (4) and are given by

$$P_{w1} = P_{w2} = \frac{N_{\text{wall}}}{N_{\text{tot}}} = \frac{\rho_w h_w}{2 \rho_w h_w + \rho_c h_c}, \quad (5)$$

and

$$P_{\text{cav}} = \frac{N_{\text{cav}}}{N_{\text{tot}}} = \frac{\rho_c h_c}{2 \rho_w h_w + \rho_c h_c}. \quad (6)$$

2.2. Fano test verification

In the simulations performed to verify the compliance with the Fano test, nuclear reactions have been switched off and secondary particles have not been followed, considering that they are locally absorbed at the points where they are generated.

The z -dependence of the absorbed dose per emitted proton has been investigated using a scoring grid composed of cylindrical voxels, covering the entire simulation phantom. These voxels have the same radius r as the phantom pieces and a height of 0.1 cm. The absorbed dose is expected to show an increase with z up to a maximum value, labeled D_{Fano} , which indicates that charged particle equilibrium has been reached. For larger z values, the absorbed dose should remain constant, equal to this maximum value.

If the condition regarding the charged particle equilibrium discussed above is satisfied, the cavity should be situated within this plateau, and the absorbed dose in the cavity per proton emitted should be:

$$D_{\text{Fano}} = \frac{E_0}{m_{\text{tot}}}, \quad (7)$$

where $m_{\text{tot}} = 2 m_w + m_c$ is the total mass of the phantom. The ratio

$$Q = \frac{D_c}{D_{\text{Fano}}}, \quad (8)$$

where D_c is the absorbed dose in the cavity, per proton emitted, obtained in the Monte Carlo simulation, has been calculated to check

whether the Fano test is verified: the further Q deviates from 1, the lower the degree of compliance with the Fano test. Q can be also written as follows:

$$Q = \frac{E_c}{m_c} \frac{2 m_w + m_c}{E_0} = \frac{E_c}{E_0} \left(1 + \frac{2 \rho_w h_w}{\rho_c h_c} \right), \quad (9)$$

where E_c is the energy deposited in the cavity, per proton emitted, estimated in the simulation.

2.3. Radiation yield and nuclear reactions

In the case of protons with the energies considered in this work, the bremsstrahlung produced is not significant. For light charged particles, bremsstrahlung is the main process contributing to radiation yield. The radiation yield represents the fraction of the total energy of a particle that is emitted in the form of radiation as it slows down while moving in a material medium. Apart from that, other non-negligible contributions to radiation yield must be taken into account: those linked to nuclear reactions, in which neutrons and photons can be produced. The situation described in the previous section, in which $Q \sim 1$ provided that the Fano test is satisfied, corresponds to simulations performed by switching off nuclear reactions and absorbing locally all secondary particles. This means that in these simulations, both nuclear and radiation yield effects have not been taken into account.

Let assume now that nuclear reactions are considered and secondary particles are transported and let D_c^{tot} be the absorbed dose in the cavity, per proton emitted, obtained in the simulation in these new circumstances. Because of the radiation production, the dose in the cavity is expected to be smaller now than in the previous simulations and one can write:

$$D_c^{\text{tot}} = D_c [1 - Y(E_0)]. \quad (10)$$

This equation defines $Y(E_0)$, the total radiation yield, produced in the conditions of the simulation, by protons with energy E_0 . Then, the radiation yield is given by:

$$Y(E_0) = 1 - \frac{D_c^{\text{tot}}}{D_c} = 1 - \frac{Q_{\text{tot}}}{Q}, \quad (11)$$

where we have defined

$$Q_{\text{tot}} = \frac{D_c^{\text{tot}}}{D_{\text{Fano}}}. \quad (12)$$

That is, it is possible to estimate the radiation yield for different proton energies, using the Monte Carlo estimation of Q_{tot} (or of D_c^{tot}) and results obtained with each simulation code can be compared.

2.4. Details of the simulations

In what follows some specific details of the simulations done in the present work with the codes PENH (Salvat, 2013; Salvat and Quesada, 2020, 2021), FLUKA (Boehlen et al., 2014; Battistoni et al., 2016) and TOPAS (Perl et al., 2012; Faddegon et al., 2020) are summarized.

The simulations performed can be gathered in two groups. First, those aiming at verifying the compliance with the Fano test. As said above, in these simulations nuclear reactions are switched off and secondary particles have not been followed. Within this group, we have first the simulations in which the optimal conditions for PENH to verify the Fano test are established. Specifically, the aim is to determine the proton tracking parameters required for this purpose.

A second set of simulations in the first group has involved the other two codes considered. In what refers to FLUKA, simulations using the optimal parameters recommended by Lourenço et al. (2019) have been conducted. These authors used a different procedure, with a different geometry, to check the verification of the Fano test in this code. In addition, different simulations have been performed with TOPAS to study the role of proton tracking parameters in the accomplishment of the

Fano test, as well as to carry out a comparison with the results quoted in the work by Wulff et al. (2018).

In the second group of simulations, nuclear reactions have been activated and all secondary particles have been transported, thus permitting a complete analysis of the role played by bremsstrahlung production and nuclear reactions on the Fano test verification. Simulations with the three codes have been conducted.

As indicated in Eq. (9), the quantity to be estimated in the Monte Carlo simulations is E_c , the energy deposited in the cavity per proton emitted from the source. In our simulations we have calculated separately the contribution of the protons emitted from each of the three cylinders conforming the simulation phantom, assuming that, within each cylinder, the source points are situated in the axis, uniformly distributed along its height. In this case, the quantity of interest is given by:

$$E_c = P_{w1} \cdot E_c^{w1} + P_{cav} \cdot E_c^{cav} + P_{w2} \cdot E_c^{w2}, \quad (13)$$

where E_c^{w1} and E_c^{w2} indicate the contributions to E_c of the protons emitted from the lower and the upper walls and E_c^{cav} that of the protons emitted from the cavity itself (see Fig. 1).

In the case of setup II, *i. e.* the one corresponding to the isotropic source, the overall symmetry guarantees that $E_c^{w1} = E_c^{w2}$ and only the simulations corresponding to one of the two walls should be carried out. In the case of the linear source (setup I), the contribution of the upper wall is expected to be negligible in comparison to that of the lower wall. This is because the only contributions to E_c^{w2} are those generated by protons that recoil after interacting in the medium (remember that in this setup all protons are emitted in the direction of the positive z -axis). This contribution should reduce as the initial energy of the emitted protons increases.

Due to the conditions that must be accomplished, the contribution E_c^{cav} is expected to be much smaller than the contribution of the lower wall in the case of the setup I, or than those of the two walls for setup II. To have an accurate value for E_c^{cav} , simulations following 10^9 initial protons have been carried out for all energies and materials.

In the simulations to estimate the wall contributions, the number of initial protons followed has been chosen in such a way that the uncertainty of Q is similar for all the energies analyzed. The number of protons followed in the simulations involving each wall are given in Table 1.

2.4.1. PENH

The last version available of PENH has been used in the present work (Salvat and Quesada, 2020, 2021). In these simulations, the material of the cavity has been generated by duplicating the corresponding material file used for the walls (Al, water or C) and changing the density value by hand. The parameter s_{max} was set to 1 cm in the walls and 0.01 cm in the cavity. In the simulations conducted to determine the proton tracking parameters for which the Fano test is verified, the parameter NISOT was set to 0 to switch off the nuclear reactions and the absorption energies of photons, electrons, positrons and neutrons were set to 1 GeV in all materials.

The three parameters governing proton transport are C_1 , C_2 and W_{cc} . C_1 controls the elastic mean free path of protons and C_2 defines the maximum average energy lost by protons between two “hard” collisions. PENH, as PENELOPE, is a class-II Monte Carlo code in which collision events of charged particles are classified as hard or soft: if the change in the movement direction and/or the energy lost by a particle in an interaction are larger or smaller than given thresholds, it is assumed that hard or soft events occur, respectively. In case of protons, the parameter W_{cc} denotes this energy threshold. The optimal values of these parameters permitting Fano test to be verified have been determined in the first group of simulations.

In the simulations performed to study the role of the nuclear reactions and the radiation production, the values of the parameters used for the various particles were those quoted in Table 2. It is worth

Table 2

Values of the simulation parameters adopted in PENH for the tracking of photons (γ), electrons (e^-) and positrons (e^+), protons (p), and neutrons (n). Note that, in the case of the simulations performed to analyze the verification of the Fano test, only the protons are transported and all secondary particles are assumed to be absorbed at the point where they are produced. Note that the values of the proton parameters are those obtained as optimal after the first group of simulations.

	γ	e^\pm	p	n
E_{abs} (keV)	50	50	1	100
C_1		0.1	0.05	0.0
C_2		0.1	0.05	0.0
W_{cc} (keV)		50	10	
W_{ct} (keV)		50		
FNABS				0.8

mentioning that the values indicated for the proton parameters are those that resulted from the previous study and that guarantee the verification of the Fano test. In this second group of simulations, NISOT was set to the number of isotopes involved in the simulation to switch on the nuclear reactions.

2.4.2. TOPAS

Simulations with TOPAS (version 3.9), running on the Geant4.10.07.p03 Simulation Toolkit (Perl et al., 2012; Faddegon et al., 2020), have been carried out. The material in the phantom walls and in the cavity has been generated with the same parameters (those characterizing Al, water or C), changing only the density value (see Section 2.1). In the simulations conducted to check the verification of the Fano test, only protons have been transported by setting `CutForAllParticles = 1000m` and `CutForProton = 0.05 mm` and not including the modules describing nuclear reactions in the physics list of the calculations. The electromagnetic physics list `g4e-standard_opt4` has been used.

Regarding the proton transport, the key parameters are `dRoverRange`, `finalRange` and `MaxStepSize`. The first one limits the step of the transported particle: the ratio between the step and the range of the particle must remain smaller than `dRoverRange`. The parameter `finalRange` is related to the absorption energy used in other Monte Carlo codes: it establishes an upper limit to the range of the particle above which its transport ends. Finally, `MaxStepSize` imposes an overall limit to the step of the transported particle, independently of its range.

Two sets of values for the key parameters have been chosen. On the one hand, the default values of `g4e-standard_opt4` have been considered: `dRoverRange = 0.1` and `finalRange = 50 μm`. On the other hand, the values suggested as optimal by Wulff et al. (2018) and Baumann et al. (2019) have been assumed: `dRoverRange = 0.05` and `finalRange = 0.1 μm`. In these simulations we have used `MaxStepSize = 0.01 cm` in the cavity and 1 cm in the walls, the same values as in the PENH calculations. In what follows these are referred as TOPAS *default* and *optimized* simulations and the corresponding values of the ratio Q are labeled as $Q_{TOPAS}^{default}$ and $Q_{TOPAS}^{optimized}$, respectively.

Due to the fact that some discrepancies with the results obtained with TOPAS by other authors have been found, some of the calculations have been repeated by using directly Geant4 and taking advantage of the example #3 provided in the code distribution. In these calculations the version Geant4.11.1 has been used with the same physics packages and the same values for the default tracking parameters as in the TOPAS simulations described above. The materials used in the simulation were created using the `G4NistManager` class.

The role of these parameters in what respect to the verification of the Fano test has been studied by doing several simulations in which their values have been changed. This has permitted also to compare with the results of previous works (Sterpin et al., 2014; Wulff et al., 2018).

A second set of simulations has been conducted to study the role of the radiation production and the nuclear reactions. In these simulations, the parameter `CutForAllParticles` has been set to its default value, 0.05 mm, `MaxStepSize` has been used with the same values as in the previous simulations for all the particles transported, the values of `dRoverRange` and `finalRange` for protons have been the same as in the previous simulations and those for electrons and positrons have been 0.003 and 1 nm, respectively. Nuclear reactions are activated by using the corresponding modules in the physics list; in our case `g4h-phy_QGSP_BIC_HP` and `g4h-phy_QGSP_BERT_HP` have been used. Neutron tracking parameters have been left at their default values. The values of `MaxStepSize` for neutrons and photons, which establish their absorption energies, were the same as those indicated above for protons.

2.4.3. FLUKA

Simulations with the CERN code `FLUKA` have been performed with the version 4-3.0 (Boehlen et al., 2014; Battistoni et al., 2016). In these simulations, the prescription of Lourenço et al. (2019) has been adopted. These authors established the optimal parameters to ensure the fulfillment of the Fano test in `FLUKA` but using a procedure with a simulation geometry different to ours. The purpose of these calculations are, first, to check the Fano test according to our procedure and, second, to study the role played by nuclear reactions and the transport of secondary particles. The cavity material was generated by means of the `MATERIAL` card, by modifying the density to the appropriate value and leaving the remaining parameters that characterize Al, water or C at their original values. In the simulations done for the verification of the Fano test, the maximum step size for the proton transport has been set to 0.01 cm and the corresponding absorption energy to 10 keV. The absorption energies of the other particles have been set to 1 GeV and nuclear reactions were switched off by setting an energy value of 1 GeV in the card `THRESHOLD`. The Q values obtained in this way have been labeled as Q_{FLUKA} .

In the simulations carried out to analyze the role of the radiation production and the nuclear reactions, the `DEFAULT` card has been used in the mode `PRECISION`. A maximum step size of 0.01 cm has been set for the transport of all particles, with absorption energies of 100 keV for photons, electron, positrons, and other particles except for neutrons, for which 10^{-5} eV has been used, and for protons, for which the same value as in the previous simulations have been considered. The maximum fraction of kinetic energy lost in a step has been set to 0.05 and the threshold for delta ray production to 100 keV.

3. Results and discussion

3.1. Optimal tracking parameters for P_{ENH}

First of all, we have established the optimal P_{ENH} tracking parameters to fulfill the Fano test. Several simulations have been conducted by varying the parameters affecting proton transport. In the simulations we have considered $C_1 = C_2 = C$. The ratio Q has been calculated as indicated in Eq. (9).

In Fig. 2a we show the results obtained by maintaining $W_{\text{cc}} = 10$ keV and varying C , whose range in P_{ENH} is between 0 and 0.2. The Q values corresponding to $C = 0.05$ (black open triangles), $C = 0.1$ (red solid squares) and $C = 0.2$ (green solid circles) are shown. We can observe that all calculations verify the Fano test within the uncertainty, independently of the value of C , for all the proton energies considered.

While Q seems to be not significantly affected by the tracking parameters C_1 and C_2 , it shows up to be strongly dependent on W_{cc} . In Fig. 2b, the ratio Q obtained for $W_{\text{cc}} = 10$ keV (black open triangles), 50 keV (red solid squares), 100 keV (green solid circles) and 500 keV (blue solid triangles), are shown for the various initial proton energies considered. These calculations have been done by maintaining $C_1 = C_2 = C = 0.05$. As can be seen, the Fano test is accomplished, within

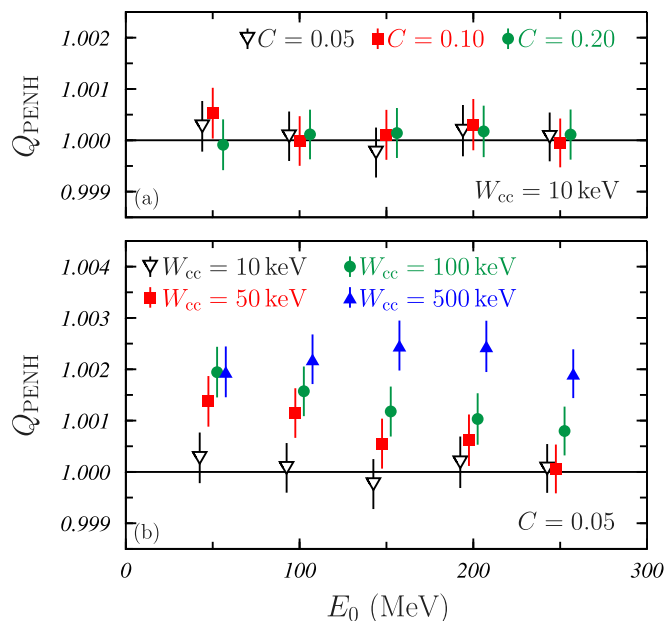


Fig. 2. The ratio Q , as defined in Eq. (8), as a function of the initial proton energy E_0 , obtained with P_{ENH} in AL. In panel (a) the results obtained for $C_1 = C_2 = C = 0.05, 0.1$ and 0.2 , maintaining $W_{\text{cc}} = 10$ keV are shown. The values in panel (b) have been found by keeping $C_1 = C_2 = C = 0.05$ and varying W_{cc} between 10 keV and 500 keV. The Q values shown with black open triangles correspond to the simulations shown in Fig. 3. Uncertainties are given with a coverage factor $k = 3$.

the uncertainties, for all energies analyzed only for $W_{\text{cc}} = 10$ keV. For the other W_{cc} values, Q approaches 1 as the energy E_0 increases, but, with the exception of the case $W_{\text{cc}} = 50$ keV for $E_0 = 250$ MeV (red solid square), and despite the values of Q differ from 1 by 0.3% at most, they are significantly different from 1 (take into account that the uncertainties shown correspond to a coverage factor $k = 3$).

Similar results were found by Sterpin et al. (2014), who analyzed the problem with a different geometry to that we have used here. For a proton beam of 100 MeV, they obtained a Q value almost independent of C_1 and C_2 for $W_{\text{cc}} = 10$ keV, while when using $C = 0.05$, Q increased with W_{cc} , reaching values above 1.005, which did not verify the Fano test even if the uncertainties of their results were larger than ours.

Here it is worth pointing out that electrons behave in a different way. Sempau and Andreo, in their work testing `PENELOPE` for the verification of the Fano test, found no significant differences by changing either W_{cc} or W_{cr} (the parameter establishing the threshold for hard/soft bremsstrahlung events). In their results, the dose in the cavity depended on the accuracy in the description of angular deflections and spatial displacements in the mixed simulation algorithm through C_1 and C_2 (Sempau and Andreo, 2006).

In the following simulations with P_{ENH} , the values $C_1 = C_2 = 0.05$ and $W_{\text{cc}} = 10$ keV have been used for protons (see Table 2). The Q values obtained in this way have been labeled as Q_{PENH} .

3.2. Charged particle equilibrium

It is worth checking that charged particle equilibrium is accomplished in the cavity. Fig. 3 shows the results obtained in the P_{ENH} (black points), `TOPAS` default (red points) and `FLUKA` (green points) simulations carried out for the 250 MeV proton beam. Note that `FLUKA` and `TOPAS` values have been shifted down 3.0 eV/g and 1.5 eV/g, respectively, to avoid the overlapping with P_{ENH} results.

In the three cases, the buildup region is clearly seen and the maximum dose is reached at $z \sim -7$ cm, far enough from the cavity, which in our simulation geometry is situated at $z \sim 0$ (see the white strip).

Similar results are obtained for the other energies using the h_w values indicated in Table 1.

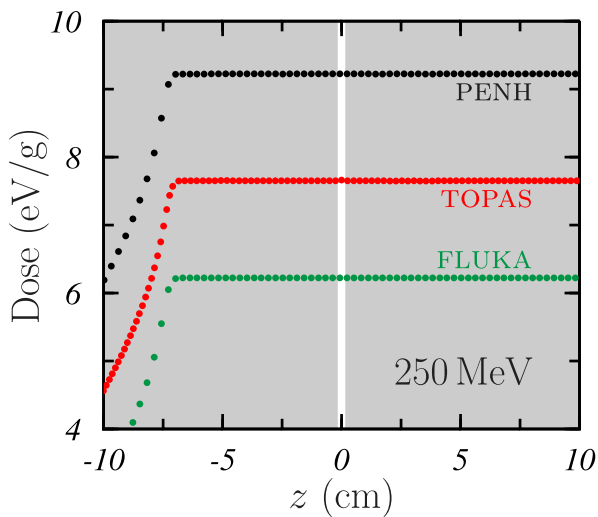


Fig. 3. Dose absorbed in the phantom as a function of z for the 250 MeV beam. The results obtained in the simulations carried out with PENH (black points), TOPAS (red points), and FLUKA (green points) are shown. The white strip represents the cavity, while the gray correspond to part of the walls. The uncertainties are smaller than the symbols used. TOPAS and FLUKA results have been shifted -1.5 eV/g and -3.0 eV/g , respectively, to avoid overlapping with PENH data.

3.3. Verification of the Fano test: linear source

The next step has been to compare how the three simulation codes considered verify the Fano test. Fig. 4 shows the Q values obtained for Al, panels (a) and (d), water, panels (b) and (e), and C, panels (c) and (f).

As it can be seen in Fig. 4a–c, both PENH (black open triangles) and FLUKA (green solid circles) satisfy the Fano test for all energies and materials considered. The optimal values of the PENH tracking parameters chosen for Al, works also well for water and C. On the other hand, it is worth recalling that FLUKA simulations have been performed with the optimal parameters recommended by Lourenço et al. (2019) and that using these values, these authors found that the test was verified for a simulation geometry very different from the one we have considered in our calculations.

TOPAS results show a different behavior. For Al (see Fig. 4d), fails in the verification of the Fano test occur for the calculations carried out using the default parameters (red open squares). Though the test is accomplished for $E_0 = 100\text{ MeV}$ and 150 MeV , a value $Q_{\text{TOPAS}}^{\text{default}} = 1.0006(5)$ has been obtained for $E_0 = 50\text{ MeV}$, whereas above 150 MeV , $Q_{\text{TOPAS}}^{\text{default}}$ grows with E_0 , reaching the value $1.0012(5)$ for the 250 MeV proton beam. The overall situation is essentially the same for $Q_{\text{TOPAS}}^{\text{optimized}}$ (red solid squares) and for the calculations carried out with the two sets of parameters in case of water (see Fig. 4e). However, worst results are obtained in both calculations for C (see Fig. 4f), with values $Q_{\text{TOPAS}}^{\text{default}} = 1.0027(4)$ and $Q_{\text{TOPAS}}^{\text{optimized}} = 1.0035(4)$ for 250 MeV protons.

Wulff et al. (2018) carried out an analysis very similar to ours. They used TOPAS (version 3.1), with Geant4.10.03.p01 and the same physics list module, g4e-standard_opt4, and they assumed default values for the tracking parameters (in their case $d\text{RoverRange} = 0.1$ and $\text{finalRange} = 20\text{ }\mu\text{m}$); also, they considered a geometry very similar to the one we have used, and water and C as materials. For the linear source Wulff et al. found Q values differing from 1 by 0.1% at most, for all the energies that they analyzed, between $E_0 = 30\text{ MeV}$ and 250 MeV .

The Q_{TOPAS} values that we have obtained for Al and water (see Fig. 4d and e, respectively) are similar to those indicated by Wulff et al. (2018): except for $E_0 = 250\text{ MeV}$, they are within 0.1% difference of $Q = 1$ (see gray band in the panels). However, for C, the results of our simulations with TOPAS, using default and optimized parameters, have

produced values of Q that are clearly above 1.001 for $E_0 \geq 150\text{ MeV}$. We have not found significant differences if $\text{finalRange} = 20\text{ }\mu\text{m}$, the default value in the calculations by Wulff et al. (2008), is used instead of $\text{finalRange} = 50\text{ }\mu\text{m}$, the value considered in our default TOPAS simulations.

Besides, it is worth pointing out that, as the uncertainties in our calculations are a factor ~ 3 smaller than those quoted by Wulff et al. (2018), we found that TOPAS does not verify the Fano test for proton energies $E_0 \geq 200\text{ MeV}$, in Al and water, and $E_0 \geq 100\text{ MeV}$, in C, and, in some cases, also for $E_0 = 50\text{ MeV}$.

Sterpin et al. (2014) found that the test was verified for 100 MeV and 250 MeV protons within 0.1% (1σ) in water. These authors considered a geometrical setup different to ours and performed the simulations directly with Geant4 (version 09.05.p02). In order to test the behavior of Geant4, the simulations described above have been repeated directly with this code, as described in Section 2.4.2. The results obtained have been plotted with red open triangles in Fig. 4d–f. As can be seen, Geant4 verifies the Fano test for all the energies analyzed and the three materials, with an accuracy very similar to that found for PENH and FLUKA. The fact that the physics and the tracking parameters used in these Geant4 calculations are the same as those considered in the TOPAS simulations, puts a doubt on the TOPAS algorithms that needs to be clarified.

To finish this subsection, the relative importance of the three contributions in Eq. (13) has been analyzed. Independently of the material considered and for $E_0 = 50\text{ MeV}$, the ratio $P_{w1} \cdot E_c^{w1} / E_c$ is 99.997%, in PENH, 99.995%, in FLUKA, and 99.998%, in TOPAS. For $E_0 \geq 100\text{ MeV}$, this ratio is bigger than 99.999% in all the codes, and grows as E_0 increases. For $E_0 = 50\text{ MeV}$, the relative contribution of the cavity, that is the ratio $P_{cav} \cdot E_c^{cav} / E_c$, is the same in the three codes: 0.0019% for Al, 0.0025% for water, and 0.0022% for C. In the simulations carried out with TOPAS, the contribution of the upper wall, $P_{w2} \cdot E_c^{w2} / E_c$ is zero in all cases studied (both for default and optimized parameters). Taking this into account, it may be concluded that the verification of the Fano test can be tested, in this setup, by only considering the emission of protons from the piece of the source that is embedded in the lower wall of the phantom.

3.4. Verification of the Fano test: isotropic source

In the case the isotropic source, the situation is more confuse. Using the default tracking parameters, Wulff et al. (2018) obtained in water the Q values shown in Fig. 5 with blue open circles. As can be seen, $Q_{\text{TOPAS}}^{\text{default}}$ grows from 1.005, for $E_0 = 30\text{ MeV}$, to 1.014, for $E_0 = 250\text{ MeV}$. These authors observed the same trend in C, with $Q_{\text{TOPAS}}^{\text{default}}$ varying between 1.003 and 1.012 in the same energy range. The uncertainties of these calculations ranged between 0.04%, for low energies, and 0.12%, for high energies, and, as a consequence, these results showed a clear violation of the Fano test at all proton energies.

To solve this drawback, Wulff et al. (2018) proposed to use $d\text{RoverRange} = 0.05$ and $\text{finalRange} = 0.1\text{ }\mu\text{m}$, the optimal values of the tracking parameters mentioned above. The Q -values that resulted from the simulations carried out were very similar for C and water. The latter are shown in Fig. 5 with blue solid circles and, as can be seen, $Q_{\text{TOPAS}}^{\text{optimized}}$ reduces from ~ 1.002 , for $E_0 = 30\text{ MeV}$, to ~ 1.001 , for $E_0 = 250\text{ MeV}$. Wulff et al. concluded that the use of these optimized parameters permitted the Fano test fulfillment at the 0.2% level. However, as can be seen in figure 3 of the paper by Wulff et al. (2018), using the uncertainties they quoted (that corresponded to a coverage factor $k = 1$), the Fano test was not verified at any of the energies they analyzed and neither for water or C: that is, the value $Q = 1$ was not statistically compatible with the results of their simulations considering these $k = 1$ uncertainties. If instead, a coverage factor $k = 3$ is assumed, as we are considering in our analysis and as it has been used to plot the data of Wulff et al. in Fig. 5 (see blue circles), the $Q_{\text{TOPAS}}^{\text{optimized}}$ values obtained by Wulff et al. (2018) verify the Fano test for $E_0 \geq 100\text{ MeV}$

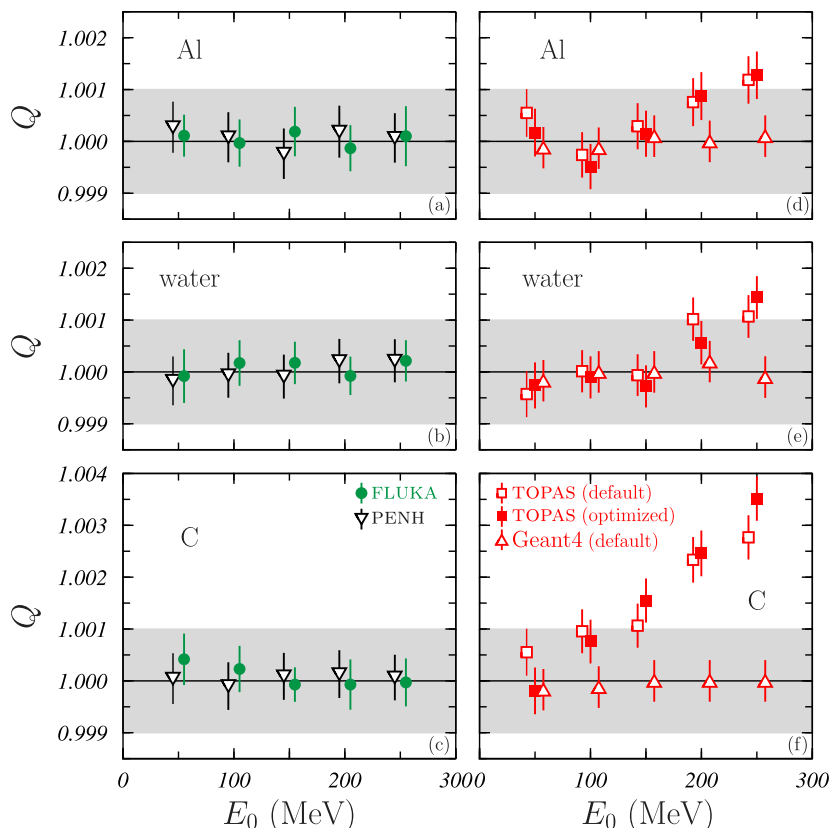


Fig. 4. The ratio Q , as defined in Eq. (8), as a function of the initial proton energy E_0 , for the linear source (setup I). Left panels show the $PENH$ (black open triangles) and $FLUKA$ (green solid circles) results, while those obtained with $Geant4$ (red solid triangles) and $TOPAS$ (red squares) are shown in right panels. Red solid squares and triangles correspond to the default tracking parameters with the physics list module `g4e-standard_opt4`, while red open squares have been obtained with the optimized parameters (see text). Upper, medium and lower panels show the Q values found for Al, water and C, respectively. Uncertainties are given with a coverage factor $k = 3$. The gray band indicates a $\pm 0.1\%$ maximum difference with respect to the expected value $Q = 1$.

in water, failing for the smaller energies. It is worth mentioning that in C, and in the same conditions, the results of Wulff et al. satisfied the test for $E_0 = 250$ MeV only.

We have simulated with $TOPAS$ the isotropic source in water, and the results obtained by using the default (optimized) tracking parameters are shown in Fig. 5 with red open (solid) squares. The behavior is quite different from that found by Wulff et al. (2018). The Q values obtained in both cases are rather similar (as it happened in the case of the linear source), all of them differ from 1 by 0.1% at most, and the test is verified for all proton energies, except in the case of the optimized parameters for 50 MeV, where $Q_{TOPAS}^{optimized} = 0.9989(8)$ and for 250 MeV, where $Q_{TOPAS}^{default} = 1.0008(6)$ for both parameter sets.

In the inset of Fig. 5, the results found for the isotropic source with $PENH$ (black open triangles) and $FLUKA$ (green solid circles). As can be seen, the results are similar to those obtained for the linear source and the test is verified by both codes for all energies with the only exception of $FLUKA$ for 50 MeV.

3.5. Role of the tracking parameters in $TOPAS$ and $Geant4$

To finish the analysis carried out, a further study of the role of the tracking parameters used in both $TOPAS$ and $Geant4$ simulations has been carried out. For this purpose, a series of simulations for different combinations of these parameters have been performed and the main result we have found is that the only parameter that affects strongly the results obtained for Q is `dRoverRange`.

In Fig. 6, Q values obtained for Al with $TOPAS$ and $Geant4$ are shown in panels (a) and (b), respectively. Therein open symbols show the results found with `dRoverRange = 0.1` (which are the same as in Fig. 4d), while those calculated with `dRoverRange = 0.01` are plotted with solid

symbols. Despite what might be expected when using a more restrictive transport parameter, it can be seen that when `dRoverRange` reduces to 0.01, $Q_{TOPAS} \sim 1.003$ and $Q_{Geant4} \sim 1.002$ are obtained for all proton initial energies and these values do not verify the Fano test. Similar results are found for `dRoverRange = 0.05`.

These results point out that below a certain value of `dRoverRange`, the tracking algorithm seems to become unstable. This instability has also been observed in $Geant4$ calculations carried out by Elles et al. (2008) for electron beams.

3.6. Radiation yield and nuclear reactions

With the values of the tracking parameters indicated in Section 2.4, complete simulations in Al have been carried out to study the role of radiation yield and nuclear reactions. The results obtained for the yield Y , defined in Eq. (11), as a function of the initial proton energy, are shown in Fig. 7. Therein the Y values found for $PENH$ and $FLUKA$ are shown with black open triangles and green solid circles, respectively. In the case of $TOPAS$, two physics modules describing the nuclear reactions have been considered: BIC and Bertini. The corresponding results have been shown with red open and solid squares, respectively.

As can be seen, the Y values are below 0.1, but are not negligible. As expected, nuclear reactions and radiation production make the theoretical value $Q = 1$ to be underestimated in actual calculations. The overall trend observed is that Y grows with E_0 showing a quadratic behavior, as indicated by the fitted second degree polynomials also plotted in Fig. 7.

The Y values obtained with $PENH$ and $TOPAS/Bertini$ are practically overlapping for all the proton energies studied. The yields found with

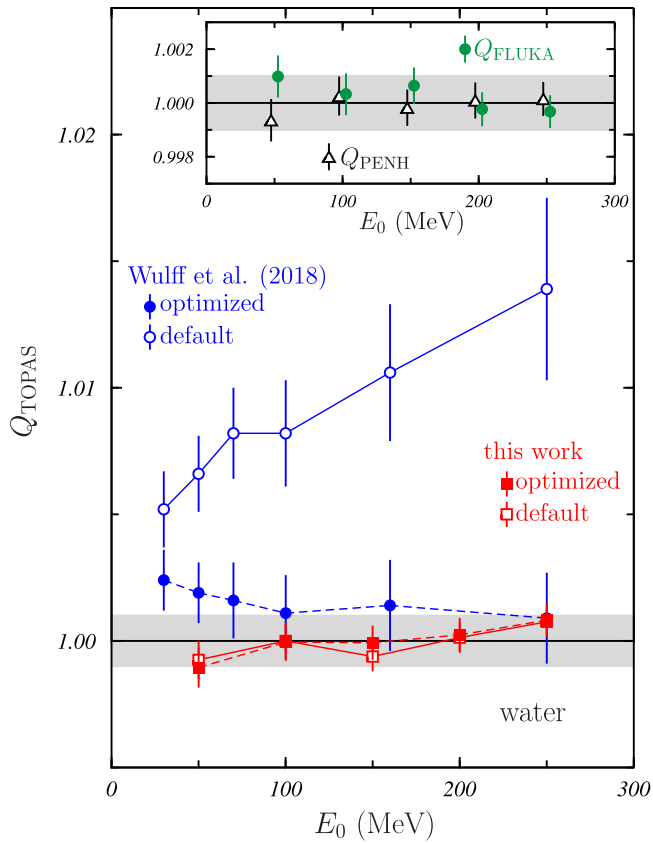


Fig. 5. The ratio Q , as defined in Eq. (8), as a function of the initial proton energy E_0 obtained with TOPAS in water for the isotropic source (setup II). Blue circles show the results quoted by Wulff et al. (2008), while red squares correspond to those found in the present work. The Q values obtained with the default (optimized) tracking parameters are shown with solid (open) symbols. Uncertainties are given with a coverage factor $k = 3$. The gray band indicates a $\pm 0.1\%$ maximum difference with respect to the expected value $Q = 1$. The lines are just joining the results corresponding to the same calculation type. In the inset, the Q values obtained for the same source with FLUKA and PENH are shown with green solid circles and black open triangles, respectively.

TOPAS/BIC are rather close to those corresponding to FLUKA. The differences between the two calculations carried out with TOPAS range between 8%, for $E_0 = 50$ MeV, and 22%, for $E_0 = 250$ MeV. The biggest values (except for 50 MeV) are those of the FLUKA simulations.

To understand the source of these yields, simulations have been carried out in which nuclear reactions are switched off but all secondary particles generated by protons in any other processes are followed. The absence of nuclear reactions strongly reduced Y : above 90% for PENH, above 95% in the case of FLUKA and between 50% and 90% in case of TOPAS (with both BIC and Bertini producing similar results). The general trend is that the reduction is larger as the initial energy of the protons increases, except for FLUKA. This indicates that the radiation yield is mainly due to nuclear reactions and the particles they generate.

4. Conclusions

In this work, the verification of the Fano test for proton beams with energies up to 250 MeV has been checked by using a phantom made of Al, water and C, and two different source types. Simulations with the Monte Carlo codes PENH, FLUKA, TOPAS and Geant4 have been carried out.

First, the optimal tracking parameters for fulfilling the Fano test in the case of PENH have been obtained. It has been found that, while C_1 and C_2 do not play a relevant role, W_{cc} results to be the key parameter: the verification of the Fano test requires a value $W_{cc} = 10$ keV or smaller.

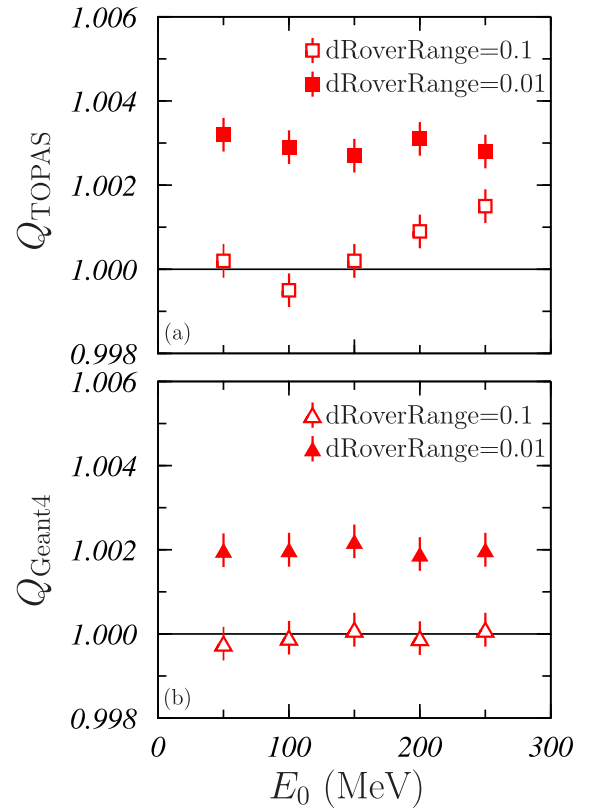


Fig. 6. The ratio Q , defined in Eq. (8), as a function of the initial proton energy E_0 , for the linear source. The results obtained with (a) TOPAS and (b) Geant4 for Al are shown. Simulations have been performed using finalRange = 0.1 μm and MaxStepSize = 0.1 mm. Open and solid symbols show the results found with dRoverRange = 0.1 and 0.01, respectively. Uncertainties correspond to a coverage factor $k = 3$.

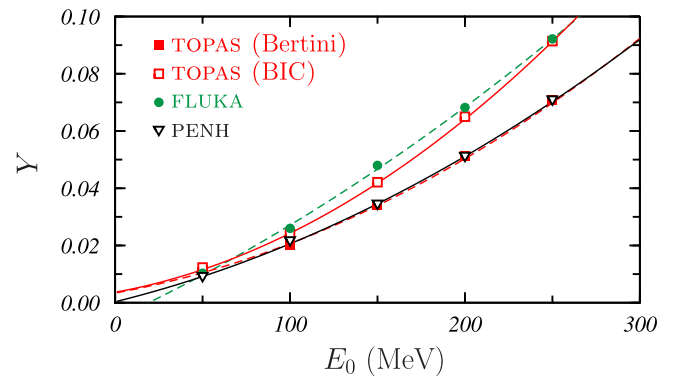


Fig. 7. Yield Y , defined in Eq. (11), as a function of the initial proton energy E_0 , obtained in simulations performed in Al with PENH (black open triangles), FLUKA (green solid circles) and TOPAS using the physics modules BIC (red open squares) and Bertini (red solid squares). Uncertainties are given with a coverage factor $k = 3$ and are smaller than the size of the symbols used.

Together with the simulations performed with PENH, the Fano test has been also checked with FLUKA and TOPAS. It has been found that, for the Al phantom, TOPAS fails to accomplish the test for energies above 150 MeV while FLUKA verifies the test at all energies. Similar results are found for the water and C phantoms. It is worth mentioning that in case of C, TOPAS results are much worse than those obtained for the other two materials, and the test is not verified for $E_0 \geq 100$ MeV. The use of optimized transport parameters proposed by Wulff et al. (2018) does not change significantly the situation. Calculations performed with

Geant4 produce results similar to those found for PENH and FLUKA, which verify the test.

The above findings correspond to a linear source emitting protons in the positive direction of the z -axis. If, instead, an isotropically emitting source is considered, similar results are found. This is in contrast to the results obtained by Wulff et al. (2018).

The important role played by the transport parameter `dRoverRange` in such calculations has been pointed out. Values of this parameter below 0.1 seem to make the tracking algorithms unstable in both TOPAS and Geant4.

The radiation yield is mainly due to nuclear reactions and results in a reduction of at most 10% of the absorbed dose in the cavity. This yield increases quadratically with the initial energy of the proton beam, irrespective of the simulation code.

CRedit authorship contribution statement

J.A. de la Torre: Conceptualization, Data curation, Formal analysis, Investigation, Methodology, Resources, Software, Validation, Visualization, Writing – original draft, Writing – review & editing. **A.M. Lallena:** Conceptualization, Data curation, Formal analysis, Funding acquisition, Investigation, Methodology, Project administration, Resources, Software, Supervision, Validation, Visualization, Writing – original draft, Writing – review & editing. **M. Anguiano:** Conceptualization, Data curation, Formal analysis, Funding acquisition, Investigation, Methodology, Project administration, Resources, Software, Supervision, Validation, Visualization, Writing – original draft, Writing – review & editing.

Declaration of competing interest

The authors declare that they have no known competing financial interests or personal relationships that could have appeared to influence the work reported in this paper.

Acknowledgments

This work has been partially supported by the Spanish Ministerio de Ciencia y Competitividad (PID2019-104888GB-I00) and Ministerio de Ciencia, Innovación y Universidades (PID2022-137543NB-I00), by the European Regional Development Fund (ERDF) and by the Junta de Andalucía (FQM387).

Data availability

Data will be made available on request.

References

Battistoni, G., Bauer, J., Boehlen, T.T., Cerutti, F., Chin, M.P.W., Augusto, R.S., Ferrari, A., Ortega, P.G., Kozłowska, W., Magro, G., Mairani, A., Parodi, K., Sala, P.R., Schoofs, P., Tessonier, T., Vlachoudis, V., 2016. The FLUKA code: an accurate simulation tool for particle therapy. *Front. Oncol.* 6, 116.

Baumann, K.-S., Horst, F., Zink, K., Gomà, C., 2019. Comparison of PENH, FLUKA and GEANT4/TOPAS for absorbed dose calculation in air cavities representing ionization chambers in high-energy photon and proton beams. *Med. Phys.* 46, 4639.

Berger, M.J., Coursey, J.S., Zucker, M.A., Chang, J., 2017. Stopping-Power and Range Tables for Electrons, Protons, and Helium Ions. NIST Standard Reference Database 124, National Institute of Standards and Technology., <https://physics.nist.gov/PhysRefData/Star/Text/PSTAR.html>.

Bielajew, A.F., Rogers, W.O., 1988. Variance-reduction techniques. In: Ettore Majorana International Science Series, vol. 38, pp. 407–420.

Boehlen, T.T., Cerutti, F., Chin, M.P.W., Fassò, A., Ferrari, A., Ortega, P.G., Mairani, A., Sala, P.R., Smirnov, G., Vlachoudis, V., 2014. The FLUKA code: developments and challenges for high energy and medical applications. *Nucl. Data Sheets* 120, 211–214.

Elles, S., Ivanchenko, V.N., Maire, M., Urban, L., 2008. Geant4 and Fano cavity test: where are we? *J. Phys.: Conf. Ser.* 102, 012009.

Erazo, F., Brualla, L., Lallena, A.M., 2014. Electron beam quality k_{Q,Q_0} factors for various ionization chambers: A Monte Carlo investigation with PENELOPE. *Phys. Med. Biol.* 59, 6673–6691.

Erazo, F., Brualla, L., Lallena, A.M., 2017. Computation of the electron beam quality k_{Q,Q_0} factors for the NE2571, NE2571A and NE2581A thimble ionization chambers using PENELOPE. *Phys. Med.* 38, 76–80.

Erazo, F., Lallena, A.M., 2013. Calculation of beam quality correction factors for various thimble ionization chambers using the Monte Carlo code PENELOPE. *Phys. Med.* 29, 163–170.

Erazo, F., Lallena, A.M., 2016. Photon beam quality correction factors for the NE2571A and NE2581A thimble ionization chambers using PENELOPE. *Phys. Med.* 32, 232–236.

Faddegon, B., Ramos-Méndez, J., Schuemann, J., McNamara, A., Shin, J., Perl, J., Paganetti, H., 2020. The TOPAS tool for particle simulation, a Monte Carlo simulation tool for physics, biology and clinical research. *Phys. Med.* 72, 114–121.

Fano, U., 1954a. Inelastic collisions and the Molière theory of multiple scattering. *Phys. Rev.* 93, 117–120.

Fano, U., 1954b. Note on the Bragg-Gray cavity principle for measuring energy dissipation. *Radiat. Res.* 1, 237–240.

Garvía, A.M., Zamora, L.L., Anguiano, M., Lallena, A.M., García-Pareja, S., 2024. Monte Carlo calculation of the photon beam quality correction factor k_{Q,Q_0} for ionization chambers of very small volume: Use of variance reduction techniques driven with an ant colony algorithm. *Radiat. Phys. Chem.* 225, 112110.

González-Castaño, D.M., Hartmann, G.H., Sánchez-Doblado, F., Gómez, F., Kapsch, R.-P., Pena, J., Capote, R., 2009. The determination of beam quality correction factors: Monte Carlo simulations and measurements. *Phys. Med. Biol.* 54, 4723–4741.

Lourenço, A., Bouchard, H., Galer, S., Royle, G., Palmans, H., 2019. The influence of nuclear interaction on ionization chamber perturbation factors in proton beams: FLUKA simulations supported by a Fano test. *Med. Phys.* 46, 885–891.

Muir, B.R., McEwen, M.R., Rogers, D.W.O., 2012. Beam quality conversion factors for parallel-plate ionization chambers in MV photon beams. *Med. Phys.* 39, 1618–1631.

Muir, B.R., Rogers, D.W.O., 2010. Monte Carlo calculations of k_Q , the beam quality conversion factor. *Med. Phys.* 37, 5939–5950.

Muir, B.R., Rogers, D.W.O., 2013. Monte Carlo calculations for reference dosimetry of electron beams with the PTW Roos and NE2571 ion chambers. *Med. Phys.* 40, 121722.

Perl, J., Shin, J., Schümann, J., Faddegon, B., Paganetti, H., 2012. TOPAS: an innovative proton Monte Carlo platform for research and clinical applications. *Med. Phys.* 39, 6818–6837.

Reis, C.Q.M., Nicolucci, P., 2016. Assessment of ionization chamber correction factors in photon beams using a time saving strategy with PENELOPE code. *Phys. Med.* 32, 297–304.

Salvat, F., 2013. A generic algorithm for Monte Carlo simulation of proton transport. *Nucl. Instrum. Methods Phys. Res. B* 316, 144–159.

Salvat, F., Quesada, J., 2020. Nuclear effects in proton transport and dose calculations. *Nucl. Instrum. Methods Phys. Res. B* 475, 49–62.

Salvat, F., Quesada, J., 2021. Collisions of nucleons with atoms: Calculated cross sections and Monte Carlo simulation. *Front. Phys.* 9, 733949.

Sempau, J., Andreo, P., 2006. Configuration of the electron transport algorithm of PENELOPE to simulate ion chambers. *Phys. Med. Biol.* 51, 3533–3548.

Spencer, L.V., 1975. Some comments on Fano's theorem. *Radiat. Res.* 63, 191–199.

Sterpin, E., Sorriax, J., Souris, K., Vynckier, S., Bouchard, H., 2014. A Fano cavity test for Monte Carlo proton transport algorithms. *Med. Phys.* 41, 011706.

Wulff, J., Baumann, K., Verbeek, N., Bäumer, C., Timmermann, B., Zink, K., 2018. TOPAS/Geant4 configuration for ionization chamber calculation in proton beams. *Phys. Med. Biol.* 63, 115013.

Wulff, J., Heverhagen, J.T., Zink, K., 2008. Monte Carlo based perturbation and beam quality corrections factors for thimble ionization chambers in high energy photon beams. *Phys. Med. Biol.* 53, 2823–2836.

Wulff, J., Heverhagen, J.T., Zink, K., Kawrakow, I., 2010. Investigation of systematic uncertainties in Monte Carlo-calculated beam quality correction factors. *Phys. Med. Biol.* 55, 4481–4493.

Zink, K., Wulff, J., 2008. Monte Carlo calculations of beam quality correction factors k_Q for electron dosimetry with a parallel-plate Roos chamber. *Phys. Med. Biol.* 53, 1595–1607.

Zink, K., Wulff, J., 2012. Beam quality corrections for parallel-plate ion chambers in electron reference dosimetry. *Phys. Med. Biol.* 57, 1831–1854.